catalysts

MDPI

Article

Promoting Electricity Production and Cr (VI) Removal Using a Light–Rutile–Biochar Cathode for Microbial Fuel Cells

Baoyin Sun [1,†], Wenqing Xie [2,†], Xiangwen Zhang [3], Yunzhu Zhou [2], Zhaolin Yang [2], Lei Wang [4], Jiqiang Zhou [4] and Guiping Ren [2,*]

1 The Second Geological and Mineral Exploration Institute of Gansu Provincial Bureau of Geology and Mineral Exploration and Development, Lanzhou 730000, China
2 The Key Laboratory of Mineral Resources in Western China (Gansu Province), School of Earth Sciences, Lanzhou University, Lanzhou 730000, China
3 The Gansu Provincial Bureau of Geology and Mineral Exploration and Development, Lanzhou 730000, China
4 Gansu Nonferrous Engineering Survey, Design and Research Institute, Lanzhou 730000, China
* Correspondence: renguiping@lzu.edu.cn
† These authors contributed equally to this work.

Abstract: Microbial fuel cell (MFC) technology holds significant promise for the production of clean energy and treatment of pollutants. Nevertheless, challenges such as low power generation efficiency and the high cost of electrode materials have impeded its widespread adoption. The porous microstructure of biochar and the exceptional photocatalytic properties of rutile endow it with promising catalytic potential. In this investigation, we synthesized a novel Rutile–Biochar (Rut-Bio) composite material using biochar as a carrier and natural rutile, and explored its effectiveness as a cathode catalyst to enhance the power generation efficiency of MFCs, as well as its application in remediating heavy metal pollution. Furthermore, the impact of visible light conditions on its performance enhancement was explored. The X-ray diffraction (XRD), X-ray photoelectron spectroscopy (XPS) and scanning electron microscopy (SEM) analysis validated the successful fabrication of rutile composites loaded with biochar. The maximum current density and power density achieved by the MFCs were 153.9 mA/m^2 and 10.44 mW/m^2, respectively, representing a substantial increase of 113.5% and 225% compared to the control group. In addition, biochar-supported rutile MFCs showed excellent degradation performance of heavy metal pollutants under light conditions. Within 7 h, the Cr^{6+} degradation rate reached 95%. In contrast to the blank control group, the removal efficiency of pollutants exhibited increases of 630.8%. The cyclic degradation experiments also showcased the remarkable stability of the system over multiple cycles. This study successfully integrated natural rutile and biochar to fabricate highly efficient cathode photocatalyst composites, which not only enhanced the power generation performance of MFCs but also presented an environmentally sustainable and economically viable method for addressing heavy metal pollution.

Keywords: heavy metal pollution; MFC; biochar; rutile; photocatalyst

Citation: Sun, B.; Xie, W.; Zhang, X.; Zhou, Y.; Yang, Z.; Wang, L.; Zhou, J.; Ren, G. Promoting Electricity Production and Cr (VI) Removal Using a Light–Rutile–Biochar Cathode for Microbial Fuel Cells. *Catalysts* **2024**, *14*, 648. https://doi.org/10.3390/catal14090648

Academic Editors: Annalisa Vacca and Ciro Bustillo-Lecompte

Received: 30 August 2024
Revised: 16 September 2024
Accepted: 19 September 2024
Published: 22 September 2024

1. Introduction

With the intensification of human activities and rapid economic development, heavy metal and organic pollution are increasingly exerting severe impacts on and causing damage to the natural environment [1–4]. One of the major concerns is the high toxicity, long-lasting nature, and slow biodegradation of heavy metal pollution. This type of pollution not only causes harm to the ecological environment but also presents a significant risk to human health through direct ingestion, inhalation of air, and skin contact [5–8]. Chromium (Cr) is inevitably used as mordants and impregnators in the impregnation industry, and if the concentration is too high, it will cause immeasurable damage to the human nervous system [9,10]. Consequently, addressing chromium pollution has become an urgent priority. The main approaches used to address heavy metals are mainly

based on physical and chemical methods. However, these physicochemical approaches are characterized by high energy consumption and limited cost-effectiveness. Moreover, biotreatment technology offers a more economical and environmentally friendly alternative; nevertheless, its efficacy is significantly constrained when dealing with heavy metals exhibiting low bioavailability [11].

The microbial fuel cell (MFC) is a novel device that utilizes oxidation–reduction reactions to transform organic chemical energy into electrical power [12,13]. In MFCs, the bacteria decompose various organic compounds and complexes of heavy metals to generate electrons and protons, which in turn enhance their respiratory system while demonstrating the ability to generate an electron flow through the electrodes [14,15]. MFC offers a cost-effective, versatile, and eco-friendly approach to eliminating heavy metal contaminants from the environment. It has the ability to simultaneously generate sustainable energy and degrade pollutants, and has received extensive attention from researchers [16–19]. Simultaneously, MFC has demonstrated significant promise in addressing the issue of heavy metal contamination [20,21]. In recent years, MFC has also played a huge role in the field of wastewater hydrogen production [22]. The efficiency of power generation in MFC development has long been a significant obstacle, mainly due to activation losses, limitations in concentration/mass transfer, and ohmic losses experienced during operation [23]. Meanwhile, microbial community is also a key factor affecting the efficiency of MFC system. Various microorganisms in the form of a community or consortium have a higher ability to transfer electrons to the anode and increase the degradation of the organic compound than pure cultures [24]. Refraining from extensive development in practical pollutant degradation applications, microbial fuel cells have yet to achieve widespread implementation [25,26]. It is crucial to enhance the expandability of MFC technology by employing inventive design and cost-efficient materials [27].

In the past few years, scientists have been working to find effective methods to enhance the electricity generation efficiency of MFCs [28]. Nevertheless, the effectiveness of MFC can be impacted by a range of constraining elements, predominantly stemming from the makeup of the electrolyte solution and the materials used for the anode and cathode [29–31]. Among a plethora of studies aimed at enhancing the efficiency of MFCs, extensive research has consistently focused on the development of electrode catalytic materials with enhanced efficacy [32,33]. The development of carbon materials and carbon-based composites has flourished in the anode of MFCs during the past few years [34]. Multiple research studies have effectively demonstrated improved reaction speeds and decreased charge transfer resistance through the application of adjustments to activated carbon cathodes [35,36]. Polypyrrole (PPy) nanotube films were synthesized by the reactive self-degradation template method as anode materials to enhance the electricity generation efficiency of MFC [37]. Zhao et al. [38] increased active sites on the cathode by oxidizing modified molybdenite. The use of the $Li_{0.95}Ta_{0.76}Nb_{0.1}9Mg_{0.15}O_3$ (LTNMg) ferroelectric cathode ceramic in the MFC device process resulted in a significant 96% reduction in COD after 168 h of operation, leading to a maximum power density of 228 mW/m^{-2} for biofuel cells [39]. Prior studies have shown that the effectiveness of battery power production is directly impacted by the conductivity, surface texture, flexibility, and compatibility with living tissue of cathode materials [40]. Due to its exceptional catalytic performance, platinum (Pt) has been widely employed as a cathode catalyst, leading to a significant improvement in the electrical output of MFCs. However, the high cost associated with platinum limits its widespread application on a large scale. As a result, scientists are presently directing their attention towards the creation of electrode catalysts using non-precious metals. Lu et al. [41] created a nitrogen-doped carbon material with pores that encase iron-based nanoparticles (Fe-Nx/C) for use as an MFC cathode catalyst, demonstrating higher catalytic activity than Pt catalysts. Nevertheless, the complex production process poses new obstacles for practical application, requiring further investigation and advancement of cathodic catalytic materials that are both cost-effective and environmentally sustainable.

In previous research, there has been considerable interest in using natural minerals as cathode catalysts to improve the power generation performance of microbial fuel cells. This is due to their widespread availability on Earth, as well as their environmentally friendly nature and ease of acquisition, especially when compared to expensive and complex synthetic materials. Ren et al. [42] employed natural hematite as a cathode catalyst, resulting in a substantial enhancement of the maximum power density in MFC. Previous studies have demonstrated the promising application potential of TiO_2, a representative semiconductor mineral, as a cathode catalyst in various fields. TiO_2 exhibits excellent electrochemical properties, facilitating electron transfer and enhancing the catalytic activity of redox reactions [43]. Sulfonated titanium dioxide (S-TiO_2) was synthesized by attaching sulfonic groups to TiO_2, and then incorporated into the PVDF-g-PSSA as a highly effective inorganic additive. This method enhances both the proton conductivity and fouling resistance of the resulting S-TiO_2/PPSSA proton exchange membrane (PEM) simultaneously [44]. Chen et al. [45] fabricated a catalytic cathode composed of CeO_2/TiO_2/ACF and paired it with a biological anode to enhance the cathodic reaction rate. Ren et al. [46] designed a one-dimensional photoanode made of titanium dioxide doped with iron oxide, which effectively enhances the electricity generation performance of MFC. However, the agglomeration of TiO_2 particles imposes certain limitations on the further enhancement of MFC performance. The biochar, an economically viable and eco-friendly porous substance, possesses numerous functional groups as well as a substantial specific surface area and porosity, making it an excellent carrier. Furthermore, its outstanding resistance to corrosion, minimal electrical resistance, and high conductivity serve to broaden its range of applications [47]. Hence, biochar is widely utilized as a support medium for electrode catalysts [48,49]. Yuan et al. [50] produced biochar from sludge and used it as a catalyst at the cathode; the MFC with sludge biochar showed the highest redox peak current. Therefore, it is crucial to synergistically combine natural rutile with biochar and study its influence on MFC performance.

Nevertheless, the clustering of TiO_2 has a notable impact on its semiconductor functionality. Furthermore, there is a paucity of research investigating the utilization of natural minerals and biochar as catalysts for MFC electrodes. In this investigation, we synthesized a novel Rutile–Biochar (Rut-Bio) composite material incorporating natural rutile into biochar. The Rut-Bio composite material was subsequently employed as the photocatalytic cathode in MFC, and its catalytic activity under visible light irradiation was assessed through analysis of the electrical properties and power output effects within the MFC system. Additionally, we examined the influence of Rut-Bio on enhancing the degradation efficiency of heavy metal contamination in MFC systems. The effect of Rut-Bio cathode catalytic material on the degradation rate of Cr^{6+} was investigated by a high-concentration degradation experiment and multiple cyclic degradation. The photocatalytic mechanism of the Rut-Bio composite was preliminarily discussed. We speculated that the multi-pore structure of biochar effectively alleviated the agglomeration problem of rutile particles, which enabled rutile to maximize its photocatalytic performance. This research offers a straightforward, eco-friendly, and economical cathode catalyst that holds significant promise for enhancing MFC power generation and remediating heavy metal contamination.

2. Results and Discussion

2.1. Characterization of Biochar, Rutile and Rut-Bio

The SEM analysis was used to observe the surface micro morphologies of biochar (Figure 1a), rutile (Figure 1b), and Rut-Bio (Figure 1c). Upon close inspection of Figure 1a, it can be observed that biochar displays a layered or fibrous arrangement. Moreover, it is worth noting that biochar possesses an abundance of pores with varying sizes. Round and oval granular types of natural rutile are shown in Figure 1b. The whole structure demonstrates a closely organized arrangement, with very few empty spaces between particles. When combined with rutile, biochar shows decreased distortion and increased crushing (Figure 1c). The typical particle size of biochar is around 30–40 μm, while Rut-Bio shows a decrease in average particle size to 10–20 μm. Upon comparison between the unmodified

biochar and the composite material, it is evident that the surface of the unmodified biochar appears coarse, whereas the surface of the biochar within the composite material exhibits a somewhat polished texture. This phenomenon arises from the close adhesion of rutile particles to the biochar surface, resulting in a modification of the biochar's microstructure. The findings demonstrate the outstanding composite effect of rutile and biochar.

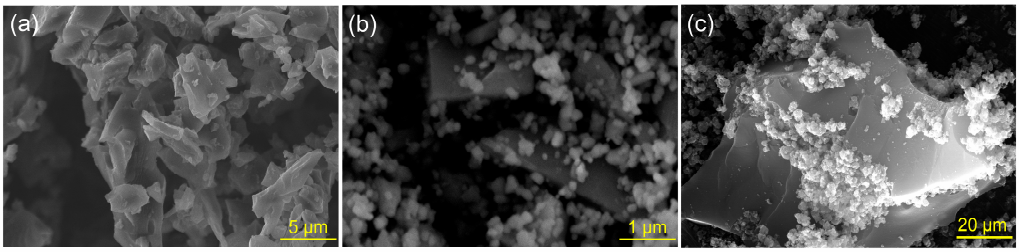

Figure 1. The SEM images of biochar (**a**), rutile (**b**) and Rut-Bio (**c**).

The results from BET analysis indicated that the nitrogen adsorption capacity of Rut-Bio was markedly superior to that of rutile, biochar, and the control group. This finding suggests that the co-doping with biochar effectively enhanced the porosity of rutile. Notably, as the pyrolysis temperature increased, the BET surface area of Rut-Bio rose significantly from 119.83 m^2/g to 267.31 m^2/g, while its total pore volume expanded from 0.12 cm^3/g to 0.35 cm^3/g, with both values being considerably higher than those for rutile and biochar alone. Therefore, it can be concluded that Rut-Bio composites demonstrate a significant enhancement in specific surface area and adsorption properties when compared to both rutile and biochar materials.

The biochar and Rut-Bio composites were subjected to XRD analysis. The XRD spectrum of the biochar exhibited three broad and gradual amorphous diffraction peaks, accompanied by several sharp and distinct minor diffraction peaks, indicating the carbonization process of the biochar (Figure 2). The crystalline compound undergoes carbonization, resulting in the formation of microcrystalline carbon with a finely graphitized particle structure. The characteristic peaks of carbon complexes appear at 26.35° and 28.24°. Following high-temperature carbonization, there is minimal alteration observed in the biochar's structure within Rut-Bio, thereby leading to negligible changes in diffraction peaks. The peaks observed at 29.63°, 36.14°, 41.82°, 48.77°, and 54.61° in the XRD pattern of the Rut-Bio composite correspond to five characteristic diffraction planes of rutile TiO_2, specifically (110), (101), (111), (200), and (211). The structural integrity and stability of Biochar–Rutile composites are very significant.

The XPS analysis provided detailed insights into the elemental composition and valence states of the sample. The full spectrum diagram reveals characteristic peaks at 284.7 eV for C 1s, 529.3 eV for O 1s, and 458.3 eV for Ti 2p in Rut-Bio composites (Figure 3a). However, the characteristic peak of Ti 2p was not discernible in the full spectrum of Biochar, indicating the successful incorporation of natural rutile into biochar. In Figure 3b, the fine spectrum of C 1s is presented, which can be resolved into five distinct carbon peaks. In addition to identifying oxidized carbon bonds such as C=O (289.1 eV) and C-O (286.7 eV), satellite peaks (π-π^*) were also detected at 293.2 eV. The appearance of C-F (295.9 eV) is typically linked to the production of biomass through its own pyrolysis process. And the weak interactions between the aromatic rings confer advantages for the adsorption of substances such as Cr, atrazine, and tetracycline [51,52]. It is noteworthy that no evident Ti-C spectral peaks were identified near 281 eV, suggesting that elemental C did not disturb the lattice of TiO_2, and confirming that anatase (TiO_2) in Rut-Bio adheres to Biochar. In the O 1s fine spectrum (Figure 3c), a distinct peak at 530.1 eV is evident for lattice oxygen (Ti-O-Ti) in anatase. The contribution of BC predominantly pertains to the hydroxyl oxygen O-H and C=O bonds. In the fine spectra of Ti 2p, as illustrated in Figure 3d, the peaks observed at 458.9 eV and 464.6 eV correspond to Ti $2p_{3/2}$ and Ti $2p_{1/2}$ of TiO_2, respectively. The energy difference between them is measured at 5.7 eV, which satisfies the valence requirement for Ti^{4+}. This provides additional evidence for the presence of Ti in the form of Ti^{4+} (TiO_2).

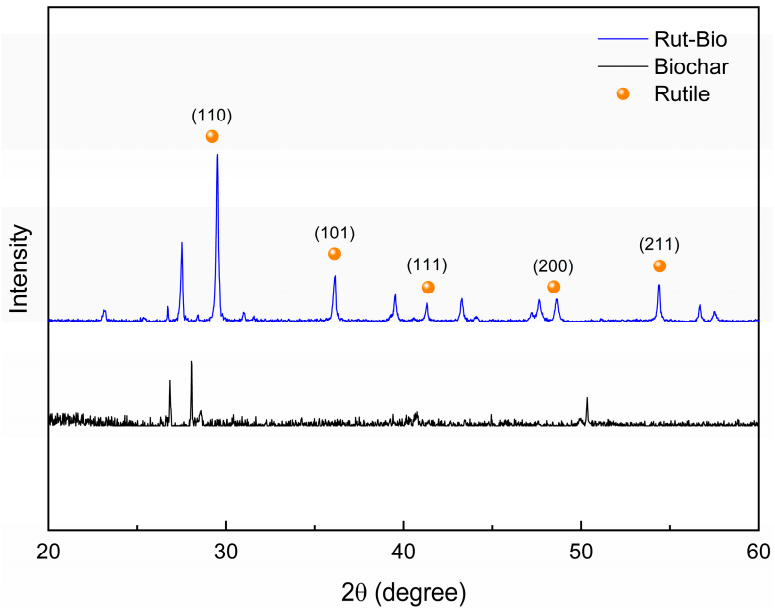

Figure 2. XRD patterns of biochar and Rut-Bio.

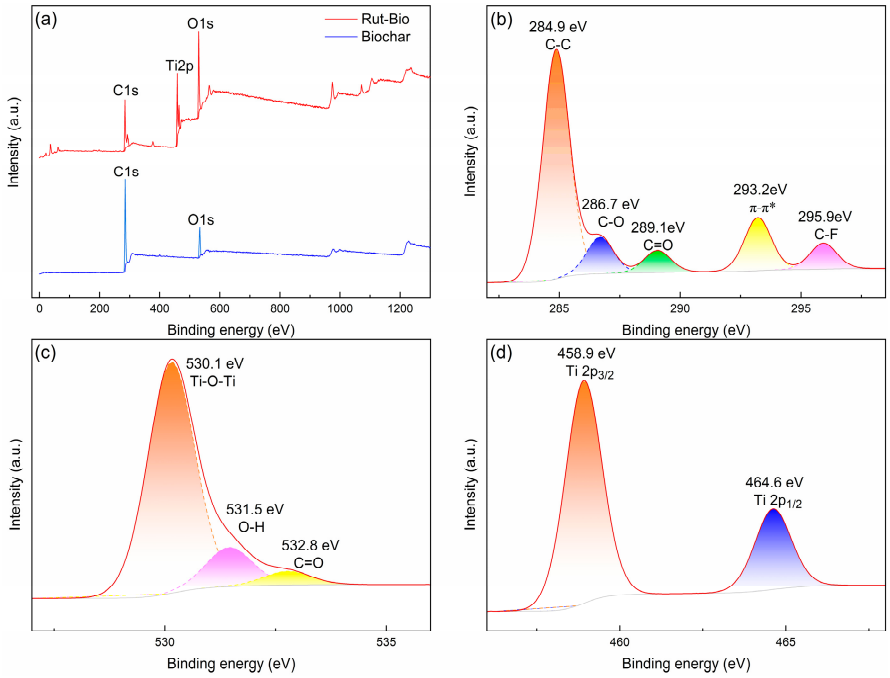

Figure 3. XPS full spectra of Rut-Bio and biochar (**a**); fine spectra of Rut-Bio on C 1s (**b**), O 1s (**c**) and Ti 2p (**d**).

2.2. Efficiency and Potential Attributes of MFC Systems

The electrode material used plays a critical role in determining the energy conversion efficiency and current density of MFC. Prior investigations have indicated that enhancing the material composition and considering the physical and chemical properties of the cathode can significantly improve both energy conversion efficiency and current density in MFCs [53]. Prior studies have indicated that the implementation of Rut-Bio composite materials as cathode catalysts yields a notable improvement in the power generation performance and output of MFC systems. Meanwhile, natural rutile minerals have been proven to have excellent photocatalytic activity [54]. Therefore, based on the comparison of the power generation performance of MFC under four different cathode materials, visible

light irradiation simulation was conducted on the Rut-Bio cathode to further explore the effect of the Rut-Bio cathode catalyst on improving the power generation efficiency of MFCs under light conditions. Figure 4a illustrates the polarization curves for each MFC system, where the linear slope signifies the charge transfer resistance [55]. The charge transfer resistance of Rut-Bio was found to be significantly lower than that of rutile and biochar, indicating a higher electron transfer rate in the Rut-Bio system. Compared with dark conditions (146.2 mA/m^2), rutile (123.6 mA/m^2), biochar (89.4 mA/m^2), and the blank control group (72.1 mA/m^2), the Rut-Bio (Light) system had a higher limit current (153.9 mA/m^2) under light conditions. Meanwhile, the maximum voltage of Rut-Bio (Light) under illumination was 345.2 mV, which was 12.4%, 53.5%, and 97% higher than that under no light conditions (307.2 mV), rutile (224.9 mV), and biochar (175.2 mV), respectively.

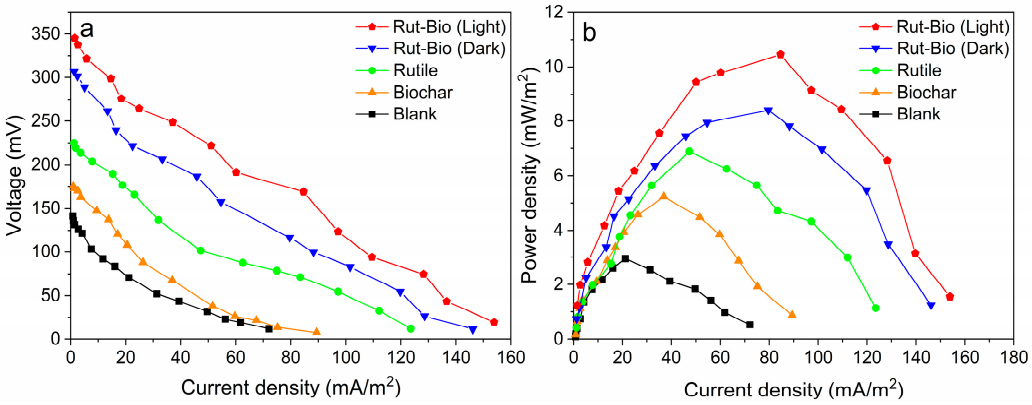

Figure 4. Polarization curves (**a**) and power density curves (**b**) of different MFCs.

The power density curve is frequently utilized to evaluate the power performance and overall power generation capacity of MFCs, achieved by adjusting the magnitude of external load resistance [56]. When the external resistance of the MFC system approached parity with the internal resistance, it led to the attainment of maximum power density. Under light conditions, the maximum power density of the Rut-Bio (Light) system increased to 10.44 mW/m^2, which was 24.1% higher than under dark conditions (8.41 mW/m^2). The peak power densities recorded for rutile and biochar were 6.89 mW/m^2 and 5.23 mW/m^2, respectively, while the control group yielded a maximum of only 2.94 mW/m^2. In comparison to the maximum power density of the control group, the Rut-Bio (Light) system demonstrated a substantial increase of 225.1%. These results indicate that Rut-Bio exhibits superior power generation performance among the four cathode materials, and its power generation capabilities are further enhanced following exposure to light in the Rut-Bio (Light) system (Table 1). When biochar-loaded rutile composite materials are exposed to light radiation, the valence band electrons transition to the conduction band, generating photo-generated electrons and leaving photo-generated holes in the valence band. The resulting photoelectron–hole pairs exhibit strong oxidation–reduction properties and undergo oxidation–reduction reactions upon reaching the catalyst surface, producing free radicals with potent oxidizing capabilities and substances with specific oxidizing abilities. Furthermore, these aforementioned free radicals and substances with strong oxidizing properties can degrade toxic pollutants into non-toxic minerals, thereby offering potential for removing heavy metal pollutants [57]. Simultaneously, there is a concurrent process of crystalline TiO_2 growth and the epitaxial carbonization of biochar, leading to the highly dispersed distribution and embedding of spherical TiO_2 particles on the biochar surface [58].

The linear fitting method was applied to analyze the ohmic polarization region of the polarization curve, and the resulting slope was utilized to determine internal resistance. Rut-Bio, rutile, and biochar demonstrated internal resistances of 3174 Ω, 3425 Ω, and 3785 Ω, respectively. Systems characterized by lower internal resistance displayed increased electron transfer capabilities and microbial degradation potential for heavy metal pollutants.

Table 1. Polarization curve and power density curve parameters.

Systems	Open Circuit Voltage (mV)	Maximum Power Density (mW/m^2)	Limiting Current Density (mA/m^2)
Rut-Bio (Light)	345.24	10.44	153.94
Rut-Bio (Dark)	307.23	9.48	146.24
Rutile	224.91	6.89	123.67
Biochar	175.26	5.23	89.45
Blank	141.32	2.94	72.14

The polarization curve and power density curve indicate that the electrical performance and power output of Rut-Bio under illumination are much higher than those of no light conditions, rutile, biochar, and blank graphite electrodes. Compared with previous studies, Rut-Bio as a cathode photocatalyst under illumination significantly improved the power generation efficiency of MFCs. In comparison to the MFC system utilizing an Fe anode and bio-cathode, which achieved a maximum power density of 1.1 mW/m^2, Rut-Bio demonstrated an increase of 849.1% [59]. Furthermore, compared to the Fe-Mn-Mg/CF composite cathode with MFCs with a maximum power density of 5.47 mW/m^2, Rut-Bio exhibited a 90.9% increase in power density [53]. Therefore, the use of biochar-loaded rutile composite materials as cathode photocatalysts represents an efficient strategy for enhancing the power generation performance of MFCs. It is noteworthy that while there is a significant improvement in power generation efficiency, the redox reaction process within MFCs is strengthened, and there may also be an enhancement in the degradation ability of heavy metal pollutants.

In order to further examine the effects of Rut-Bio cathode material and visible light on the electrode potential of the MFC system, variations in external circuit resistance were utilized to generate electrode potential curves for both the anode and cathode within the experimental setup. The anodic potential curve of Rut-Bio (Light) demonstrates a lower slope in comparison to other systems, indicating the ability of the anode to maintain a reduced potential over an extended duration (Figure 5a). Furthermore, the initial anode potential of Rut-Bio (Light) (−344 mV) is notably lower than that observed in other systems. In summary, the Rut-Bio cathode-catalysed MFC system consistently maintains a high potential with low polarization, and the anode exhibits strong electron transfer capability. Moreover, the cathode potential curve illustrates that the initial cathode potential of Rut-Bio (Light) reaches up to 1.2 mV (Figure 5b). The cathode potential curve slope of the Rut-Bio (Light) system is notably the lowest, indicating a low polarizability and excellent electron acceptance ability. The results demonstrate that utilizing the Rut-Bio composite as a cathode photocatalyst effectively increases the electrode potential difference in MFC, thereby enhancing its electron transfer rate. A higher electron transfer rate also facilitates redox reactions [60].

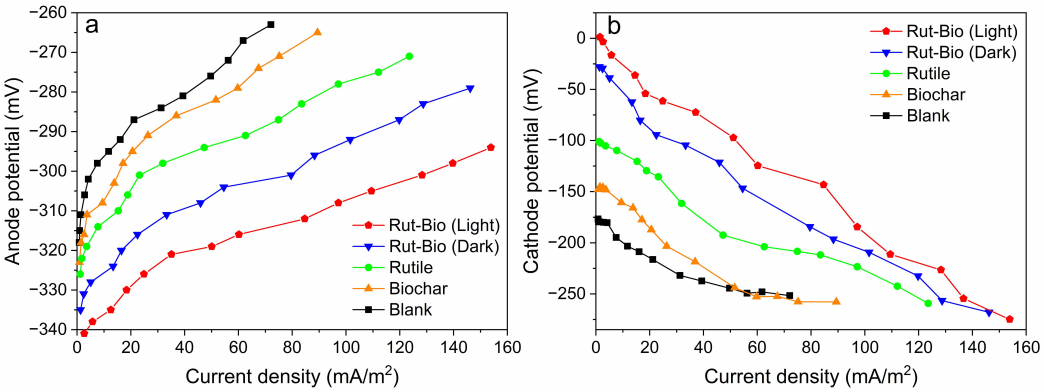

Figure 5. Anode potential curves (**a**) and cathode potential curves (**b**) of different MFCs.

2.3. Investigation of Heavy Metal Pollution Degradation by MFC

The electricity generation performance of MFCs has been demonstrated to exhibit a positive correlation with its efficiency in degrading pollutants [36]. In previous studies, it has been confirmed that Rut-Bio composite materials demonstrate a significant improvement in the degradation efficiency of heavy metal pollutants, and have great potential in the application of environmental pollution control. With the significant improvement of MFC power generation capacity by Rut-Bio (Light), we chose Cr^{6+} as indicators to evaluate heavy metal pollution and conducted in-depth research on the specific impact of Rut-Bio (Light) on the treatment effect of heavy metal pollution in order to further optimize the application of Rut-Bio composite materials in the field of environmental remediation. Under uniform experimental conditions, the degradation experiment was replicated three times to mitigate potential errors and sporadic factors. Figure 6a illustrates the degradation curves of Cr^{6+} using different MFCs, with an initial concentration of the Cr^{6+} solution set at 80 mg/L. After the experiment lasted for 7 h, the degradation efficiency of the Rut-Bio (Light) system reached 95%, which was 21.8% higher than the Rut-Bio (Dark) system with a removal rate of 78%. The degradation efficiency of rutile and biochar reached 51% and 27%, respectively. Compared to the 13% of the blank group, the degradation efficiency of the other three MFCs increased by 500%, 292.3%, and 107.7%, respectively. Obviously, the Rut-Bio composite material significantly improves the degradation efficiency of MFCs towards Cr^{6+}, and has the best effect in all four MFCs, while its degradation effect is even stronger under light conditions.

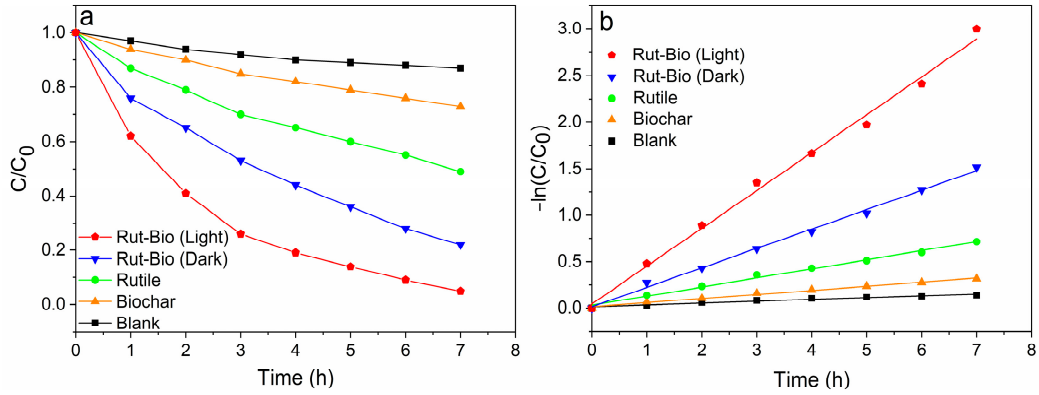

Figure 6. Degradation curve (**a**) and kinetic fitting curve (**b**) of Cr^{6+}.

We further utilized the correlation between the natural logarithm of (C/C_0) and reaction time to replicate the experimental kinetic equation (Figure 6b). In this context, C_0 denotes the initial concentration of Cr^{6+}, C represents the concentration of Cr^{6+} at a specific reaction time, and k is defined as the degradation rate constant [61]. Clearly, the Rut-Bio composite material demonstrates a fitting curve with a high slope, indicating that its degradation rate constant is notably elevated. The degradation rate constant of Rut-Bio (Light) was as high as 0.40663, significantly higher than that without illumination (0.20893). Meanwhile, the reaction rate constants of rutile (0.09745), biochar (0.04396), and the blank control group (0.01961) were all lower than those of Rut-Bio composite materials (Table 2). This further substantiates that, in the presence of light, Rut-Bio acts as a photocatalyst and significantly amplifies the degradation rate of Cr^{6+} by MFCs.

In the final phase of the experiment, we assessed the total organic carbon (TOC) levels across four distinct microbial fuel cell (MFC) systems. The TOC removal rates for each group were recorded at 15.27%, 16.81%, 23.62%, and 28.76%, respectively. Notably, the TOC removal rate in the Light-Rut-Bio system was significantly higher than that observed in other experimental groups, exhibiting an increase of 88.34% compared to the control group. This enhancement is primarily attributed to the growth and metabolic activity of microorganisms that decompose macromolecular insoluble organic matter in soil into soluble small organic acids. These organic acids serve as preferred carbon sources and

energy substrates for electrogenic microorganisms, thereby further enhancing their activity and efficiency in electricity production.

Table 2. Parameters for fitting the reaction dynamics in the system (Cr^{6+}).

Systems	Fitting Equation	Reaction Rate Constant (K/d^{-1})	R^2
Rut-Bio (Light)	y = 0.04520 + 0.40663·x	0.40663	0.9926
Rut-Bio (Dark)	y = 0.01497 + 0.20893·x	0.20893	0.9937
Rutile	y = 0.03198 + 0.09745·x	0.09745	0.9964
Biochar	y = 0.01527 + 0.04396·x	0.04396	0.9911
Blank	y = 0.01444 + 0.01961·x	0.01961	0.9951

2.4. Investigation of the Cyclic Degradation Behavior of MFC

The experimental findings demonstrate that the use of Rut-Bio composites as cathode catalysts can significantly enhance the degradation efficiency of Cr^{6+} in MFCs. Simultaneously, owing to the photocatalytic effect of natural rutile, the degradation efficiency is further enhanced under light conditions. To comprehensively assess its broad applicability and long-term stability in practical heavy metal pollution remediation, a series of five consecutive cycles of experiments were conducted. After each round of degradation, the pollutants were replenished to restore the concentration to its initial level, followed by subsequent rounds of degradation experiments. The experimental results of cyclic degradation are shown in Figure 7. Obviously, there is little change in the time of each degradation cycle. It is noteworthy that, following three cycles of degradation, the removal rate in the subsequent two cycles decreased. Nevertheless, the overall degradation rate of the system remained essentially unchanged. The Rut-Bio composite material serves as a cathode catalyst, effectively enhancing MFC performance in degrading heavy metal pollutants while demonstrating exceptional cyclic degradation stability. This outstanding cyclic degradation stability implies that the material can be efficiently recycled and reused multiple times for practical wastewater treatment applications, thereby providing a cost-effective and environmentally friendly approach to remediating heavy metal pollution. Considering the favourable photocatalytic performance of natural rutile, the material is capable of maintaining excellent catalytic performance and degradation rate under visible light.

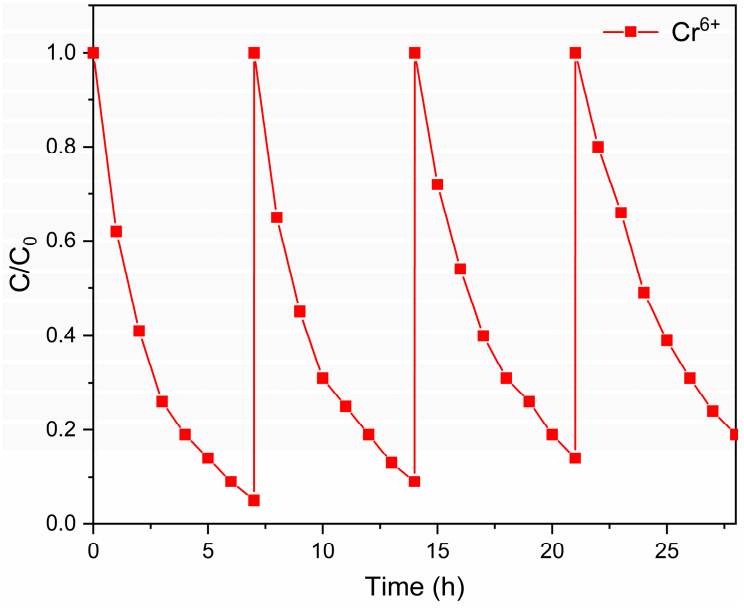

Figure 7. Cyclic degradation curves of Cr^{6+}.

2.5. Mechanism of Rut-Bio Cathode Catalysis

Figure 8 illustrates the operational mechanism of Rut-Bio composite material in enhancing the electricity generation efficiency and heavy metal removal rate within the MFC system. TiO_2 is classified as a semiconductor mineral with a band gap in the range of 3.0–3.2 eV. The Ti (IV) site situated on the surface of the TiO_2 crystal captures conduction electrons, leading to reduction to the Ti (III) state. Oxygen (O_2) molecules adsorbed on the cathode surface of MFCs undergo a reaction with the Ti (III) centre, resulting in the generation of superoxide free radicals (O_2^-). This process enhances the oxygen reduction reaction at the cathode and promotes power generation in MFCs [62]. Moreover, when compared to other metal oxide semiconducting materials, rutile displays a higher degree of Ti-O bond polarity. This characteristic facilitates the polarization and dissociation of water molecules adsorbed on its surface, resulting in the formation of hydroxyl groups [63,64]. In the liquid medium, the presence of surface hydroxyl groups can enhance the performance of TiO_2 and facilitate the adsorption of charged molecules through static electricity, leading to the formation of a diffuse electric double layer that increases electron retention capacity [65].

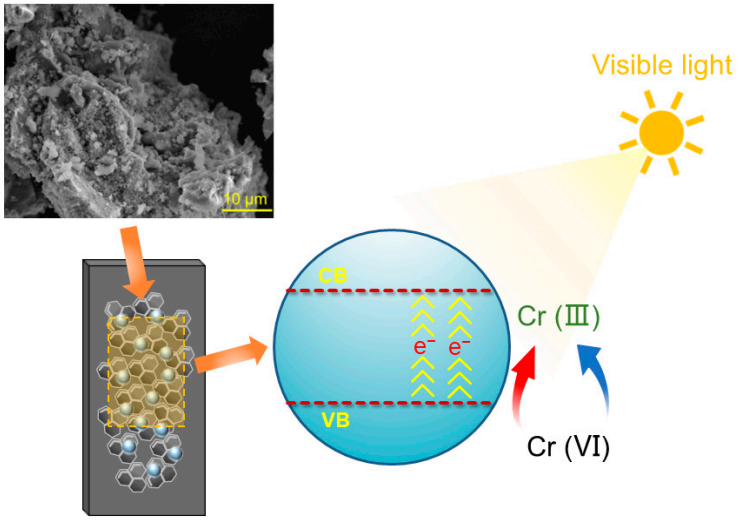

Figure 8. Schematic diagram of catalytic performance improvement in Rut-Bio.

Biochar-impregnated rutile prevents the agglomeration of rutile and significantly enhances the catalytic performance of the cathode. Furthermore, owing to its graphite-like structure and the presence of quinoline-like redox active groups, biochar possesses abundant active sites and unsaturated electron pairs [66], enabling biochar to expedite electron transfer and promote pollutant reduction transformation. Consequently, this leads to an improvement in the reaction rate at the MFC cathode and enhances pollutant removal efficiency [67]. In addition, biochar is created under high-temperature conditions, resulting in a substantial presence of pyrrolic, graphitic, and pyridinic nitrogen species that can effectively function as cathode catalysts to facilitate electron transfer at the cathode [68].

3. Materials and Methods

3.1. Preparation of Biochar and Rut-Bio Composites

The corn cobs were obtained from Ningxia, China, and underwent a 5-day sun-drying process before being finely ground into powder. Following this, the resulting powder was carefully placed in an environment enriched with nitrogen gas at a controlled intake flow rate of 0.5 L/min to create an anaerobic setting. The biochar was generated by subjecting the powder to a heating rate of 5 °C/min in a muffle furnace, maintaining a temperature of 350 °C for a duration of 2 h. Subsequently, the biochar underwent sieving through a 200-mesh sieve and was stored in a dry glass container. Natural rutile was pulverized into powder and sieved through 200 mesh screens. The Rut-Bio composite was prepared by incorporating 25% (by mass) rutile into biochar and subjecting it to oxygen-limited

pyrolysis at 500 °C, while maintaining other conditions consistent with the preparation of biochar. The mass ratio of rutile and biochar in the Rut-Bio composite material was 1:3. The resulting compounds were subsequently pulverized, passed through a 200-mesh sieve, and stored in dry glassware for future use.

3.2. Characterization of Cathode Materials

The fundamental microstructure of materials is commonly depicted using scanning electron microscopy (SEM, JSM-6510, Jeol, Tokyo, Japan. The SEM was utilized to observe the micro-morphologies of biochar and Rut-Bio at 10 kV, with a working distance of 10 mm. The structures and compositions of rutile, biochar, and Rut-Bio composites were examined using X-ray diffraction (XRD) analysis conducted on an Ultima IV X-ray diffractometer (Rigaku Corporation, Tokyo, Japan). The scanning range was configured from 10° to 80° with a scanning rate of 4° per minute. The elemental composition and valence state of Rut-Bio composite material were determined by X-ray photoelectron spectroscopy (XPS), using He lamp ultraviolet photoelectron spectroscopy (UPS) with a 6 kV argon (Ar) ion gun and Al/Mg double anode (Thermo, Waltham, MA, USA), with a maximum power of 600 W.

3.3. Construction of MFC

The experimental configuration utilized a two-chamber MFC. The anode chamber was tightly sealed with a rubber diaphragm, and a graphite anode measuring 3.5 cm × 6.0 cm was employed. The two chambers were separated by a proton exchange membrane from Du Pont Company, Wilmington, DE, USA. To explore the impact of rutile on biochar catalysis, we set up four MFCs with varying cathodes, including a graphite electrode as the baseline, an electrode coated with natural rutile, an electrode coated with biochar, and an electrode coated with Rutile–Biochar (Rut-Bio). Simultaneously, to further investigate the photocatalytic effect of visible light on Biochar–Rutile composites, an additional experimental group (Rut-Bio-Light) was established to subject the Rut-Bio cathode MFC to continuous irradiation using a self-assembled laboratory light source.

The control group comprised a standard graphite electrode, while the other three experimental groups were prepared using a two-step process. To prepare the experimental group, 0.3 mL of polytetrafluoroethylene and a small quantity of ethanol were added to 0.3 g of rutile, biochar, and Rut-Bio, and stirred until gelation occurred. Subsequently, the gel was applied to a graphite electrode (Hongfeng Carbon, Shanghai, China) sized at 3.5 cm × 6 cm with a thickness of 5 mm in order to generate a thin mineral film approximately 0.2 mm thick. Following that, the film was air-dried for 12 h at room temperature before four sets of MFCs were cultured in an incubator maintained at 35 °C.

Each anodic chamber was filled with a Luria-B (LB) medium containing 10 g/L of tryptophan, 5 g/L of yeast extract, and 10 g/L of NaCl. Soil samples containing microbial communities gathered from Yinchuan in Ningxia Province were positioned at the base of every anode chamber. Each cathode chamber was furnished with a 1.7 mm diameter aperture to ensure optimal air contact, while the cathode electrolyte comprised a 0.1 M KCl solution. Within each MFC, a titanium wire was integrated into the circuit and an external circuit was connected to a 1000 Ω resistor for electronic transmission, facilitating voltage measurement.

Substrate samples weighing 5 g were collected from four groups of MFCs. Each sample was mixed with 10 mL of water and subjected to ultrasonic treatment for 30 min to extract the biofilm adhered to the substrate surface. Following ultrasonic treatment, the substrate was washed three times, after which it was transferred into a centrifugal tube. The tube was centrifuged at 10,000 rpm for 15 min, and the resulting sediment was collected and dried at 65 °C. The sediment was then ground into a powder with a particle size of 200 mesh. The total organic carbon (TOC) content of the matrix was analyzed using a TOC analyzer (Nicolet iS50, Thermo, Waltham, MA, USA).

3.4. Degradation Performance Test of Heavy Metal Pollution

After establishing a stable condition in the MFCs equipped with four different cathodes, solutions containing 80 mg/L of Cr^{6+} were separately introduced to replace the cathode solution. Hourly samples were gathered from the cathode chamber for concentration measurement. The concentration of Cr (VI) was determined using a UV–Vis spectrophotometer and the 1,5-diphenylcarbazide method. Sample concentrations were determined based on standard curves that correlated Cr^{6+} concentrations with absorbance values. The concentrations of Cr^{6+} in the cathode chamber were measured at a pH of 2.0 under ambient temperature conditions (25 ± 2 °C).

4. Conclusions

In this study, we successfully engineered an innovative Light–Rutile–Biochar (Rut-Bio) cathode MFC system, which exhibited exceptional catalytic performance under visible light exposure leading to significant enhancements in both electrochemical properties and power generation capabilities within MFCs. Furthermore, our exploration into Rut-Bio's impact on degrading heavy metal pollutants within MFC systems revealed its remarkable efficacy through biodegradation experiments, showcasing heightened rates for Cr^{6+} even at elevated concentrations. Notably, our system displayed robust cyclic stability across multiple degradation cycles, indicating its potential for practical application. We posit that leveraging biochar-supported rutile can effectively mitigate challenges associated with particle agglomeration while offering a direct pathway towards an eco-friendly and economically viable cathode catalyst with substantial promise for augmenting MFC power output and addressing heavy metal contamination concerns. Based on simulated indoor experiments simulating heavy metal pollutant degradation processes, we intend to explore real-world applications involving more complex pollution scenarios moving forward, while concurrently refining synthesis methods aimed at minimizing costs associated with composite photocatalytic materials.

Author Contributions: Conceptualization, B.S. and W.X.; methodology, B.S. and X.Z.; validation, Y.Z., Z.Y., L.W. and J.Z.; formal analysis, B.S. and W.X.; investigation, B.S., W.X., X.Z., Y.Z., Z.Y., L.W. and J.Z.; writing—original draft preparation, B.S., W.X. and G.R.; writing—review and editing, X.Z. and G.R. All authors have read and agreed to the published version of the manuscript.

Funding: This work was supported by the Natural Science Foundation of Gansu Province, China (Grant No. 23JRRA1083), the Gansu Nonferrous Geological Bureau Research Project (Grant No. YSJG2023-13 and No. YSJD2022-11), the Fundamental Research Funds for the Central Universities (Grant No. lzujbky-2023-05 and lzujbky-2024-ou17), the Key Laboratory of Strategic Mineral Resources of the Upper Yellow River and the Ministry of Natural Resources (Grant No. YSMRKF202214).

Data Availability Statement: The original contributions presented in the study are included in the article, further inquiries can be directed to the corresponding author.

Conflicts of Interest: The authors declare no conflicts of interest.

References

1. Drinčić, A.; Zuliani, T.; Ščančar, J.; Milačič, R. Determination of hexavalent Cr in river sediments by speciated isotope dilution inductively coupled plasma mass spectrometry. *Sci. Total Environ.* **2018**, *637–638*, 1286–1294. [CrossRef] [PubMed]
2. Li, Q.; Dong, M.; Li, R.; Cui, Y.; Xie, G.; Wang, X.; Long, Y. Enhancement of Cr (VI) removal efficiency via adsorption/photocatalysis synergy using electrospun chitosan/g-C_3N_4/TiO_2 nanofibers. *Carbohydr. Polym.* **2020**, *253*, 117200. [CrossRef]
3. Gao, Q.; Tao, D.W.; Qi, Z.B.; Liu, Y.F.; Guo, J.; Yu, Y. Amidoxime functionalized PVDF-based chelating membranes enable synchronous elimination of heavy metals and organic contaminants from wastewater. *J. Environ. Manag.* **2022**, *318*, 115643. [CrossRef]
4. Maiti, S.; Ghosh, N.; Mandal, C.; Das, K.; Dey, N.; Adak, M.K. Responses of the maize plant to chromium stress with reference to antioxidation activity. *Braz. J. Plant Physiol.* **2012**, *24*, 203–212. [CrossRef]
5. Dytlow, S.; Gorka-Kostrubiec, B. Concentration of heavy metals in street dust: An implication of using different geochemical background data in estimating the level of heavy metal pollution. *Environ. Geochem. Health* **2021**, *43*, 521–535. [CrossRef] [PubMed]

6. Yang, Q.; Li, Z.; Lu, X.; Duan, Q.; Huang, L.; Bi, J. A review of soil heavy metal pollution from industrial and agricultural regions in China: Pollution and risk assessment. *Sci. Total Environ.* **2018**, *642*, 690–700. [CrossRef]
7. Shaikh, A.; Mishra, S.P.; Mohapatra, P.; Parida, S. One-step solvothermal synthesis of TiO_2-reduced graphene oxide nanocomposites with enhanced visible light photoreduction of Cr (VI). *J. Nanopart. Res.* **2017**, *19*, 206. [CrossRef]
8. Briffa, J.; Sinagra, E.; Blundell, R. Heavy metal pollution in the environment and their toxicological effects on humans. *Heliyon* **2020**, *6*, e04691. [CrossRef]
9. Jeong, H.; Lee, Y.; Moon, H.; Ra, K. Characteristics of metal pollution and multi-isotopic signatures for C, Cu, Zn, and Pb in coastal sediments from special management areas in Korea. *Mar. Pollut. Bull.* **2023**, *188*, 114642. [CrossRef]
10. Qin, X.; Bai, L.; Tan, Y.; Li, L.; Song, F.; Wang, Y. β-Cyclodextrin-crosslinked polymeric adsorbent for simultaneous removal and stepwise recovery of organic dyes and heavy metal ions: Fabrication, performance and mechanisms. *Chem. Eng. J.* **2019**, *372*, 1007–1018. [CrossRef]
11. Rajendran, S.; Priya, T.A.K.; Khoo, K.S.; Hoang, T.K.A.; Ng, H.S.; Munawaroh, H.S.H.; Karaman, C.; Orooji, Y.; Show, P.K. A critical review on various remediation approaches for heavy metal contaminants removal from contaminated soils. *Chemosphere* **2021**, *287*, 132369. [CrossRef] [PubMed]
12. Yaqoob, A.A.; Ibrahim, M.N.M.; Guerrero-Barajas, C. Modern trend of anodes in microbial fuel cells (MFCs): An overview. *Environ. Technol. Innov.* **2021**, *23*, 101579. [CrossRef]
13. Lovley, D. Bug juice: Harvesting electricity with microorganisms. *Nat. Rev. Microbiol.* **2006**, *4*, 487–508. [CrossRef] [PubMed]
14. Bazina, N.; Ahmed, T.G.; Almdaaf, M.; Jibia, S.; Sarker, M. Power generation from wastewater using microbial fuel cells: A review. *J. Biotechnol.* **2023**, *374*, 17–30. [CrossRef]
15. Malik, S.; Kishore, S.; Dhasmana, A.; Kumari, P.; Mitra, T.; Chaudhary, V.; Kumari, R.; Bora, J.; Ranjan, A.; Minkina, T.; et al. A Perspective Review on Microbial Fuel Cells in Treatment and Product Recovery from Wastewater. *Water* **2023**, *15*, 316. [CrossRef]
16. Daud, N.N.M.; Ahmad, A.; Yaqoob, A.A.; Ibrahim, M.N.M. Application of rotten rice as a substrate for bacterial species to generate energy and the removal of toxic metals from wastewater through microbial fuel cells. *Environ. Sci. Pollut. Res.* **2021**, *28*, 62816–62827. [CrossRef]
17. Patel, A.; Choi, Y.; Sim, S. Emerging prospects of mixotrophic microalgae: Way forward to sustainable bioprocess for environmental remediation and cost-effective biofuels. *Bioresour. Technol.* **2020**, *300*, 122741. [CrossRef]
18. AlSayed, A.; Soliman, M.; Eldyasti, A. Microbial fuel cells for municipal wastewater treatment: From technology fundamentals to full-scale development. *Renew. Sustain. Energy Rev.* **2020**, *134*, 110367. [CrossRef]
19. Idris, S.A.; Esat, F.N.; Abd Rahim, A.A.; Rizzqi, W.A.Z.; Ruzlee, W.; Razali, W.M.Z. Electricity generation from the mud by using microbial fuel cell. *MATEC Web Conf.* **2016**, *69*, 02001. [CrossRef]
20. Li, W.; Yu, H.; Zhen, H. Towards sustainable wastewater treatment by using microbial fuel cells-centered technologies. *Energy Environ. Sci.* **2014**, *7*, 911–924. [CrossRef]
21. Mian Chen, B.Y.; Tobias, M.B.; Rakan, M.A.; Peter, G.P. Composition Dependence of Ethanol Oxidation at Ruthenium. *J. Electrochem. Soc.* **2018**, *165*, J3019–J3025. [CrossRef]
22. Arun, J.; SundarRajan, P.; Pavithra, K.G.; Priyadharsini, P.; Shyam, S.; Goutham, R.; Le, Q.H.; Pugazhendhi, A. New insights into microbial electrolysis cells (MEC) and microbial fuel cells (MFC) for simultaneous wastewater treatment and green fuel (hydrogen) generation. *Fuel* **2024**, *355*, 129530. [CrossRef]
23. Aelterman, P.; Rabaey, K.; Pham, H.T.; Boon, N.; Verstraete, W. Continuous electricity generation at high voltages and currents using stacked microbial fuel cells. *Environ. Sci. Technol.* **2006**, *40*, 3388–3394. [CrossRef] [PubMed]
24. Meylani, V.; Surahman, E.; Fudholi, A.; Almalki, W.H.; Ilyas, N.; Sayyed, R.Z. Biodiversity in microbial fuel cells: Review of a promising technology for wastewater treatment. *J. Environ. Chem. Eng.* **2023**, *11*, 109503. [CrossRef]
25. Shi, L.; Dong, H.L.; Reguera, G.; Beyenal, H.; Lu, A.H.; Liu, J.; Yu, H.Q.; Fredrickson, J.K. Extracellular electron transfer mechanisms between microorganisms and minerals. *Nat. Rev. Microbiol.* **2016**, *14*, 651–662. [CrossRef]
26. Katuri, K.P.; Kalathil, S.; Ragab, A.; Bian, B.; Alqahtani, M.F.; Pant, D.; Saikaly, P.E. Dual-function electrocatalytic and macroporous hollow-fiber cathode for converting waste streams to valuable resources using microbial electrochemical systems. *Adv. Mater.* **2018**, *30*, e1707072. [CrossRef]
27. Pandit, S.; Savla, N.; Jung, S. Recent advancements in scaling up microbial fuel cells. In *Integrated Microbial Fuel Cells for Wastewater Treatment*; Butterworth-Heinemann: Oxford, UK, 2020; pp. 349–368.
28. Badi, N.; Theodore, A.M.; Alghamdi, S.A.; Al-Aoh, H.A.; Lakhouit, A.; Roy, A.S.; Ignatiev, A. Fabrication and Characterization of Flexible Solid Polymers Electrolytes for Supercapacitor Application. *Polymers* **2022**, *14*, 3837. [CrossRef]
29. Jung, S.; Mench, M.M.; Regan, J.M. Impedance characteristics and polarization behavior of a microbial fuel cell in response to short-term changes in medium pH. *Environ. Sci. Technol.* **2011**, *45*, 9069–9074. [CrossRef]
30. Jung, S. Impedance analysis of geobacter sulfurreducens PCA, shewanella oneidensis MR-1, and their coculture in bioeletrochemical systems. *Int. J. Electrochem. Sci.* **2012**, *7*, 11091–11100. [CrossRef]
31. Kang, H.; Jeong, J.; Gupta, P.L.; Jung, S.P. Effects of brush-anode configurations on performance and electrochemistry of microbial fuel cells. *Int. J. Hydrogen Energy* **2017**, *42*, 27693–27700. [CrossRef]
32. Logan, B.E.; Hamelers, B.; Rozendal, R.; Schröder, U.; Keller, J.; Freguia, S.; Aelterman, P.; Verstraete, W.; Rabaey, K. Microbial fuel cells: Methodology and technology. *Environ. Sci. Technol.* **2006**, *40*, 5181–5192. [CrossRef] [PubMed]

33. Zhou, M.; Chi, M.; Luo, J. An overview of electrode materials in microbial fuel cells. *J. Power. Sources* **2011**, *196*, 4427–4435. [CrossRef]
34. Fan, X.; Zhou, Y.; Jin, X.; Song, B.; Li, Z.; Zhang, Q. Carbon material-based anodes in the microbial fuel cells. *Carbon Energy* **2021**, *3*, 449–472. [CrossRef]
35. Koo, B.; Jung, S.P. Improvement of air cathode performance in microbial fuel cells by using catalysts made by binding metal-organic framework and activated carbon through ultrasonication and solution precipitation. *Chem. Eng. J.* **2017**, *424*, 130388. [CrossRef]
36. Koo, B.; Lee, S.; Oh, S.; Kim, E.J.; Hwang, Y.; Seo, D.; Kim, J.Y.; Kahng, Y.H.; Lee, Y.W.; Chung, S.; et al. Addition of reduced graphene oxide to an activated-carbon cathode increases electrical power generation of a microbial fuel cell by enhancing cathodic performance. *Electrochim. Acta* **2019**, *297*, 613–622. [CrossRef]
37. Zhao, C.; Wu, J.; Kjelleberg, S.; Loo, J.S.C.; Zhang, Q. Employing a flexible and low-cost polypyrrole nanotube membrane as an anode to enhance current generation in microbial fuel cells. *Small* **2015**, *11*, 3440–3443. [CrossRef]
38. Zhao, X.; Ke, Z.; Wang, Q. Efficient organic contaminant and Cr (VI) synchronous removing by one-step modified molybdenite cathode microbial fuel cells. *Environ. Sci. Pollut. Res.* **2023**, *30*, 4423–4434. [CrossRef] [PubMed]
39. Touach, N.; Benzaouak, A.; Toyir, J.; El Hamidi, A.; El Mahi, M.; Lotfi, E.M.; Kacimi, M.; Liotta, L.F. Bioenergy Generation and Wastewater Purification with $Li_{0.95}Ta_{0.76}Nb_{0.19}Mg_{0.15}O_3$ as New Air-Photocathode for MFCs. *Catalysts* **2022**, *12*, 1424. [CrossRef]
40. Xu, H.T.; Wang, L.G.; Wen, Q.; Chen, Y.; Qi, L.J.; Huang, J.X.; Tang, Z.S. A 3D porous NCNT sponge anode modified with chitosan and polyaniline for high-performance microbial fuel cell. *Bioelectrochemistry* **2019**, *129*, 144–153. [CrossRef]
41. Lu, G.L.; Zhu, Y.L.; Lu, L.; Xu, K.L.; Wang, H.M.; Jin, Y.H.; Ren, Z.J.; Liu, Z.N.; Zhang, W. Iron-rich nanoparticle encapsulated, nitrogen doped porous carbon materials as efficient cathode electrocatalyst for microbial fuel cells. *J. Power Sources* **2016**, *315*, 302–307. [CrossRef]
42. Ren, G.P.; Ding, H.R.; Li, Y.; Lu, A.H. Natural hematite as a low-cost and earth-abundant cathode material for performance improvement of microbial fuel cells. *Catalysts* **2016**, *6*, 157. [CrossRef]
43. Zlámalová, M.; Lásková, P.; Vinarčíková, M.; Zukalová, M. Inherent electrochemical activity of TiO_2 (anatase, rutile) enhances the charge capacity of cathodes of lithium-sulfur batteries. *J. Solid State Electrochem.* **2022**, *26*, 639–647. [CrossRef]
44. Li, C.; Song, Y.; Wang, X.; Zhang, Q. Synthesis, characterization and application of S-TiO_2/PVDF-g-PSSA composite membrane for improved performance in MFCs. *Fuel* **2020**, *264*, 116847. [CrossRef]
45. Chen, Q.; Liu, L.; Liu, L.; Zhang, Y. A novel UV-assisted PEC-MFC system with CeO_2/TiO_2/ACF catalytic cathode for gas phase VOCs treatment. *Chemosphere* **2020**, *255*, 126930. [CrossRef]
46. Ren, G.P.; Sun, Y.; Lu, A.H.; Li, Y.; Ding, H.R. Boosting electricity generation and Cr (VI) reduction based on a novel silicon solar cell coupled double-anode (photoanode/bioanode) microbial fuel cell. *J. Power Sources* **2018**, *408*, 46–50. [CrossRef]
47. Cai, T.; Huang, M.H.; Huang, Y.X.; Zheng, W. Enhanced performance of microbial fuel cells by electrospinning carbon nanofibers hybrid carbon nanotubes composite anode. *Int. J. Hydrogen Energy* **2019**, *44*, 3088–3098. [CrossRef]
48. Chang, H.; Gustave, W.; Yuan, Z. One-step fabrication of binder-free air cathode for microbial fuel cells by using balsa wood biochar. *Environ. Technol. Innov.* **2020**, *18*, 100615. [CrossRef]
49. Ramya, M.; Harsha, V.K.; Senthil, K.P. Metal mixed biochar electrodes for the generation of electricity with high power density in microbial fuel cell. *Sustain. Energy Technol. Assess.* **2022**, *53*, 102549. [CrossRef]
50. Yuan, Y.; Yuan, T.; Wang, D.; Tang, J.H.; Zhou, S.G. Sewage sludge biochar as an efficient catalyst for oxygen reduction reaction in a microbial fuel cell. *Bioresour. Technol.* **2013**, *144*, 115–120. [CrossRef]
51. Cheng, Y.; Wang, B.; Shen, J.; Yan, P.; Kang, J.; Wang, W.; Bi, L.; Zhu, X.; Li, Y.; Wang, S.; et al. Preparation of novel N-doped biochar and its high adsorption capacity for atrazine based on π-π electron donor-acceptor interaction. *J. Hazard. Mater.* **2022**, *432*, 128757. [CrossRef]
52. Chen, M.; Yan, Z.; Luan, J.; Sun, X.; Liu, W.; Ke, X. π-π electron-donor-acceptor (EDA) interaction enhancing adsorption of tetracycline on 3D PPY/CMC aerogels. *Chem. Eng. J.* **2023**, *454*, 140300. [CrossRef]
53. Wang, W.Y.; Zhao, Q.L.; Ding, J.; Wang, K.; Jiang, J.Q. Development of an MFC-powered BEF system with novel Fe–Mn–Mg/CF composite cathode to degrade refractory pollutants. *J. Clean. Prod.* **2021**, *326*, 129348. [CrossRef]
54. Chuan, X.; Lu, A.; Chen, J.; Li, N.; Guo, Y. Microstructure and photocatalytic activity of natural rutile from China for oxidation of methylene blue in water. *Mineral. Petrol.* **2008**, *93*, 143–152. [CrossRef]
55. Liao, Z.; Sun, J.; Sun, D.; Si, R.; Yong, Y. Enhancement of power production with tartaric acid doped polyaniline nanowire network modified anode in microbial fuel cells. *Bioresour. Technol.* **2015**, *192*, 831–834. [CrossRef] [PubMed]
56. Ma, H.; Zheng, Y.; Xian, J.; Feng, Z.; Li, Z.; Cui, F. A light-enhanced α-FeOOH nanowires/polyaniline anode for improved electricity generation performance in microbial fuel cells. *Chemosphere* **2022**, *296*, 133994. [CrossRef]
57. Han, B. *Study on Modification of Rutile TiO_2 and Its Photocatalytic Activity Mechanism*; Jilin University: Changchun, China, 2022.
58. Chen, J.; Zhang, W.; Li, X.; Huang, R.; Liu, Q.; Zhang, Y.; Gan, T.; Huang, Z.; Hu, H. Mutually supportive growth strategy to engineer a hollow biochar sphere-supported TiO_2 composite with improved interfacial compatibility for efficient visible light-driven photocatalysis. *J. Environ. Chem. Eng.* **2023**, *11*, 110327. [CrossRef]
59. Wang, R.; Wan, S.; Liu, B. Denitrification in perspective of carbon neutralization: CO_2 emission reduction and electricity generation by Fe-anode and bio-cathode MFC. *J. Water Process Eng.* **2022**, *48*, 102868. [CrossRef]

60. Li, C.; Liu, Y.; Luo, M.; Cao, J.; Fang, F.; Feng, Q.; Luo, J.; Hao, L.; Wang, C. Enhancing simultaneous electrosynthesis of CO_2 and nitrogen removal in microbial fuel cell (MFC) cathode compartment by adding Fe–C/biochar compound substrates. *J. Power Sources* **2023**, *560*, 232707. [CrossRef]
61. Liu, R.; Liu, J.; Kong, W.; Huang, H.; Han, X.; Zhang, X.; Liu, Y.; Kang, Z. Adsorption dominant catalytic activity of a carbon dots stabilized gold nanoparticles system. *J. Dalton Trans.* **2014**, *43*, 10920–10929. [CrossRef]
62. Bhowmick, G.D.; Das, S.; Ghangrekar, M.M.; Mitra, A.; Banerjee, R. Improved wastewater treatment by combined system of microbial fuel cell with activated carbon/TiO_2 cathode catalyst and membrane bioreactor. *J. Inst. Eng. India Ser. A* **2019**, *100*, 675–682. [CrossRef]
63. Li, Y.; Liu, L.; Yang, F. Destruction of tetracycline hydrochloride antibiotics by FeOOH/TiO_2 granular activated carbon as expanded cathode in low-cost MBR/MFC coupled system. *J. Membr. Sci.* **2017**, *525*, 202–209. [CrossRef]
64. Liu, C.; Min, Y.; Zhang, A.; Si, Y.; Chen, J.; Yu, H.Q. Electrochemical treatment of phenol-containing wastewater by facet-tailored TiO_2: Efficiency, characteristics and mechanisms. *Water Res.* **2019**, *165*, 114980. [CrossRef] [PubMed]
65. Zhao, J.; Cheng, L.; Wang, J.; Liu, Y.Y.; Yang, J.; Xu, Q.Z.; Chen, R.S.; Ni, H.W. Heteroatom-doped carbon nanofilm embedded in highly ordered TiO_2 nanotube arrays by thermal nitriding with enhanced electrochemical activity. *J. Electroanal. Chem.* **2019**, *852*, 113513. [CrossRef]
66. Zhang, Z.K.; Zhu, Z.Y.; Shen, B.X.; Liu, L.N. Insights into biochar and hydrochar production and applications: A review. *Energy* **2019**, *171*, 581–598. [CrossRef]
67. Li, Y.; Li, H.; Huang, W. Research progress on the biochar production and its applications in enhancing electron transport and catalysis performance. *Res. Environ. Sci.* **2021**, *34*, 1157–1167.
68. Liang, B.; Li, K.; Liu, Y.; Kang, X. Nitrogen and phosphorus dual-doped carbon derived from chitosan: An excellent cathode catalyst in microbial fuel cell. *Chem. Eng. J.* **2019**, *358*, 1002–1011. [CrossRef]